Impact of donor halogenation on reorganization energies and voltage losses in bulk-heterojunction solar cells

Wu, Hongbo; Ma, Zaifei; Li, Mengyang; Lu, Hao; Tang, Ailing; Zhou, Erjun; Wen, Jin; Sun, Yanming; Tress, Wolfgang; Olsen, Jógvan Magnus Haugaard

Total number of authors:
13

Published in:
Energy & Environmental Science

Link to article, DOI:
10.1039/D3EE00174A

Publication date:
2023

Document Version
Peer reviewed version

Energy & Environmental Science

Accepted Manuscript

This article can be cited before page numbers have been issued, to do this please use: H. Wu, Z. Ma, M. Li, H. Lu, A. Tang, E. Zhou, J. Wen, Y. Sun, W. Tress, J. M. H. Olsen, S. Meloni, Z. Bo and Z. Tang, *Energy Environ. Sci.*, 2023, DOI: 10.1039/D3EE00174A.

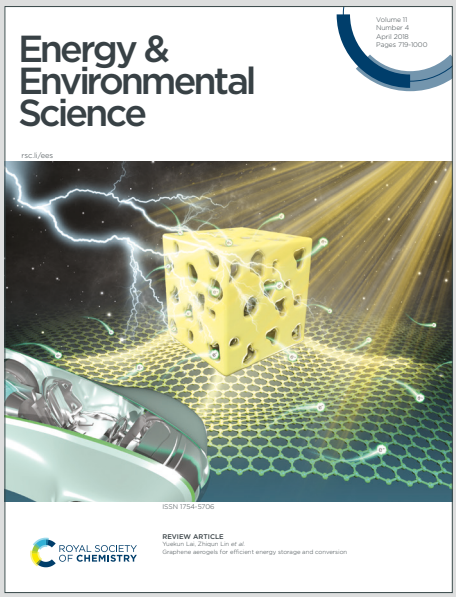

ROYAL SOCIETY OF CHEMISTRY

rsc.li/ees

DOI: 10.1039/D3EE00174A

Impact of Donor Halogenation on Reorganization Energies and Voltage Losses in Bulk-heterojunction Solar Cells

Hongbo Wu[1], Zaifei Ma[1,*], Mengyang Li[1], Hao Lu[2], Ailing Tang[3], Erjun Zhou[3], Jin Wen[1], Yanming Sun[4], Wolfgang Tress[5], Jógvan Magnus Haugaard Olsen[6], Simone Meloni[7,*], Zhishan Bo[2,*], Zheng Tang[1,*]

[1.]State Key Laboratory for Modification of Chemical Fibers and Polymer Materials, Center for Advanced Low-dimension Materials, College of Materials Science and Engineering, Donghua University, 201620 Shanghai, P. R. China
[2.]Key Laboratory of Energy Conversion and Storage Materials, College of Chemistry, Beijing Normal University, 100875, Beijing, P. R. China
[3.]CAS Center for Excellence in Nanoscience National Center for Nanoscience and Technology, 100190 Beijing, P. R. China
[4.]School of Chemistry, Beihang University, 100191 Beijing, P. R. China
[5.]Institute of Computational Physics, Zurich University of Applied Sciences, Wildbachstr. 21, 8401 Winterthur, Switzerland
[6.]DTU Chemistry, Technical University of Denmark, DK-2800 Kongens Lyngby, Denmark
[7.]Dipartimento di Scienze Chimiche, Farmaceutiche e Agrarie – DOCPAS, University of Ferrara, Ferrara, Italy

***Corresponding authors**
mazaifei@dhu.edu.cn (Zaifei Ma)
mlnsmn@unife.it (Simone Meloni)
zsbo@bnu.edu.cn (Zhishan Bo)
ztang@dhu.edu.cn (Zheng Tang)

Keywords: organic solar cell; bulk-heterojunction; donor halogenation; voltage loss; reorganization energy

Abstract

Donor halogenation is a common molecular design strategy used to reduce voltage losses (ΔV_{loss}) and improve the power conversion efficiency (PCE) of bulk-heterojunction (BHJ) organic solar cells. Here, the impact of donor halogenation on the performance of organic donor-acceptor (DA) solar cells based on over 30 different materials systems is investigated, and the main reason for the improved performance of solar cells after donor halogenation is ascribed to the increased energy of charge transfer (CT) state, and the reduced reorganization energy of the CT states (λ_{CT}). Also, the impact of donor halogenation on λ_{CT} is found to be stronger for the solar cells using the

Y-series acceptors (Y5, Y6, etc.) than those using the non-Y-series acceptors (fullerene, ITIC, etc.), which is conducive to achieving lower ΔV_{loss} in organic solar cells. Finally, the impact of donor halogenation on the solar cell performance is demonstrated to be dependent on the halogen substitution position, as well as the number of halogen atoms added to the donor molecule: Halogen substitution on the side groups of the donor molecule is found to be more effective than substitution at the backbone in reducing ΔV_{loss}. These results suggest that future molecular design strategies focusing on the reduction of materials reorganization energy will be of great importance for further improving the performance of organic solar cells.

1. Introduction

The performance of bulk-heterojunction (BHJ) organic solar cells has been improving rapidly over the past years, and the power conversion efficiencies (PCEs) of the most efficient organic solar cells are now over 19%,[1–6] owing to the development of highly efficient donor and acceptor materials via tailored molecular design strategies.[7–10] One important method to improve the optoelectronic properties of the active materials is to employ the halogenation strategy.[11–15] It has been demonstrated that using halogenated donor materials,[13,16,17] instead of non-halogenated ones, results in the better aligned energy levels of the donor-acceptor (DA) blend systems, giving rise to higher photovoltaic quantum efficiency.[18,19] Furthermore, solar cells constructed using halogenated donors were also observed to have significantly lower non-radiative recombination voltage loss (ΔV_{nr}), associated with higher external quantum efficiency of electroluminescence (EQE_{EL}).[20–23] Consequently, the overall voltage loss (ΔV_{loss}) is lower,[21,23] and the open-circuit voltage (V_{OC}) is higher in organic solar cells based on halogenated donors, as compared to those based on non-halogenated donors.

ΔV_{nr} in organic solar cells originates from strong vibrational coupling between the ground state and the charge transfer (CT) states formed at the DA interfaces,[24–26] which in a simplified model linearly reduces with increasing energy of the CT state (E_{CT}), following the so-called energy gap law.[24,27] Thus, the lower ΔV_{nr} in the solar cells based on halogenated donors can partly be attributed to the higher E_{CT},[24] resulting from the lowering of the highest occupied molecular orbital (HOMO) level. However, the reduction in ΔV_{nr} in organic solar cells after donor halogenation is

View Article Online
DOI: 10.1039/D3EE00174A

often considerably higher than what is predicted by the energy gap law, especially in the case of solar cells based on the Y-series acceptors like Y5,[28] Y6,[29] and Y7[30]: ΔV_{nr} of the BHJ devices based on fluorinated donor PM6 or chlorinated donor PM7,[31,32] mixed with Y6, was only about 0.25 V,[33] and thus significantly lower than that based on the non-halogenated PBDB-T:Y6 system (0.35 V),[34] although the difference in E_{CT} was less than 0.05 eV (E_{CT} of the blends based on PM6:Y6 and PBDB-T:Y6 were found to be 1.31 and 1.33 eV, respectively).[35]

Later, it was found that reducing the energetic driving force, defined as the difference between E_{CT} and the energy of the singlet excited state (S_1) of the pristine donor or acceptor, could lead to a hybridization between the CT and the S_1 state. The hybridization gives rise to an increased CT to ground transition dipole moment and increased EQE_{EL}.[36] Thus, the smaller driving force, due to the higher E_{CT} of the blend systems based on halogenated donors, could be an additional reason for the increased EQE_{EL} and reduced ΔV_{nr}. However, in this case, the reduced ΔV_{nr} should be associated with increased radiative recombination voltage loss (ΔV_r).[24,35,36] This is contrary to that observed for the solar cells after donor halogenation: Both ΔV_{nr} and ΔV_r are lower in the solar cells based on halogenated donors, compared to those based on non-halogenated donors.[22,23] Therefore, the origin of the impact of donor halogenation on the performance, especially voltage losses in organic solar cells, is still not fully understood. Understanding the reason behind the reduction in ΔV_{loss} after donor halogenation is expected to be of great importance for the development of molecular design strategies for more efficient organic photovoltaic materials, and thus, for breaking through the performance bottleneck of organic solar cells.

In this study, over 30 DA systems were analyzed and it was found that the reduction in ΔV_{loss} in solar cells after donor halogenation is attributed to the suppressed geometric reorganization of the organic blend materials, resulting in a lower CT state reorganization energy (λ_{CT}). Additionally, the reduction in ΔV_{loss} was shown to be restricted in blend systems using non-Y series acceptors (such as ITIC,[37] IT4F,[38] IT4Cl,[39] etc.). Because donor halogenation, despite being able to reduce the reorganization energy of the donor (λ_D), leads to an increased reorganization energy of acceptor (λ_A) for the blends based on the non-Y series acceptors. On the other hand, for the solar cells based on the Y-series acceptors (Y5, Y6, Y7, etc.), donor halogenation reduces the λ_D without affecting λ_A. This explains the more significant impact of donor halogenation on ΔV_{loss} for the solar cells

based on the Y-series acceptors, as compared to those based on the non-Y-series acceptors. Finally, the impact of the donor halogenation strategy on λ_{CT}, as well as ΔV_{loss} of the solar cells, is found to be dependent on the number of halogen atoms added and the halogen substitution position on the donor molecule. These results not only shed light on the mechanism behind the reduction in ΔV_{loss} in BHJ solar cells after donor halogenation, but also highlight the critical role played by molecular reorganization in determining the V_{OC} of these solar cells. As voltage losses are the main obstacle to achieving higher PCEs in organic solar cells, minimizing this issue through molecular structural engineering to reduce the reorganization energy is a promising direction for future research aimed at enhancing the performance of organic solar cells.

2. Results and discussion

2.1. Analysis of voltage losses in organic solar cells based on halogenated and non-halogenated donors

To evaluate the impact of donor halogenation on voltage losses, we first constructed solar cells based on a non-halogenated donor, namely, PBDB-T,[40] and halogenated donors including PM6 and PM7.[31,32] Different acceptor materials were used, and the device architecture was ITO/ZnO/active layer/MoO_3/Ag. Chemical structures of the active materials used are provided in **Figure S1 (Note S1**, **ESI)**. First, the absorption and photoluminescence (PL) spectra of the acceptors are measured to determine their bandgap energy (E_g),[41] as shown in **Figure S2 (Note S2**, **ESI)**. The E_g values of the acceptor materials are used as the representative E_g of the blend active layers, since the bandgap of the acceptor is always smaller than that of the donor in the blends studied in this work. Then, current density-voltage (*J-V*) measurements are performed to determine the basic photovoltaic performance parameters of the solar cells. The results are shown in **Figure S3 and Table S1 (Note S3**, **ESI)**. Sensitive photovoltaic external quantum efficiency (EQE_{PV}) measurements (**Figure S4**, **ESI**) are also conducted on these solar cells to calculate $V_{oc,rad}$, the radiative limit for V_{OC} (details regarding the determination of $V_{oc,rad}$ are provided in **Note S4**, **ESI**). **Figure 1**a illustrates the overall voltage losses (ΔV_{loss}), defined as the difference between $\frac{E_g}{q}$ and V_{oc} (where q is the elementary charge), plotted as a function of $V_{oc,rad}$, for the solar cells based on the Y-series (Y5, Y6, Y7), as well as the non-Y series acceptors (fullerene, ITIC, etc).

From **Figure 1a**, the first thing noted is that the $V_{oc,rad}$ of the solar cells based on the Y-series acceptors are generally lower than that based on the non-Y-series acceptors. This is mainly due to the smaller E_g of the Y-series acceptors (<1.45 eV), giving rise to a much higher value for the ideal dark saturation current density ($J_{0,rad}$, details are provided in **Note S4**, **ESI**). More importantly, ΔV_{loss} is found to be generally lower in solar cells based on halogenated donors, regardless of the acceptor used (Figure 1a), with the degree of reduction in ΔV_{loss} in solar cells based on Y-series acceptors being about 17-26%, which is higher than that based on non-Y-series acceptors (about 10-20%).

From the above results, both ΔV_{nr} and ΔV_r of the solar cells are expected to reduce after donor halogenation, and the impact of the donor halogenation strategy on ΔV_{loss} is expected to be stronger for the solar cells based on the Y-series acceptors.

Then, ΔV_r and ΔV_{nr} are determined using the following equations

$$\Delta V_r = \frac{E_g}{q} - V_{oc,rad} \quad (1)$$

$$\Delta V_{nr} = V_{oc,rad} - V_{oc} \quad (2)$$

As shown in **Figure 1b,** ΔV_{nr} of the solar cells are indeed considerably lower in the solar cells based on halogenated donors. The reduced ΔV_{nr} suggests that EQE_{EL} increases after donor halogenation,[42] since

$$\Delta V_{nr} = -\frac{kT}{q}\ln(EQE_{EL}) \quad (3)$$

where k is the Boltzmann constant, T is temperature. This is confirmed by the measurements of EQE_{EL}: The emission efficiency of the solar cells based on halogenated donors is much higher, by as much as two orders of magnitude, compared to that based on non-halogenated donors, as shown in **Figure 1c**. The increase in EQE_{EL} leads to a reduction in ΔV_{nr}, and the ΔV_{nr} values derived from EQE_{EL} agree well with those determined from $V_{oc,rad}$. Furthermore, ΔV_r of the solar cells based on halogenated donors is also found to be lower **(Figure 1d**), which suggests that the radiative decay rate of CT state (k_r) is reduced after donor halogenation,[25] since in organic solar cells, ΔV_r reduces with reducing k_r,[24,43,44]

$$\Delta V_r = -\frac{kT}{q}\ln\left(\frac{\alpha}{k_r}\right) \quad (4)$$

where α is related to the generation rate of CT states. Accordingly, the increased EQE_{EL} ($\approx \frac{k_r}{k_{nr}}$),

and thus the reduced ΔV_{nr}, after donor halogenation, must mainly be a result of reduced non-radiative decay rate of CT state (k_{nr}).[24,26,45,46]

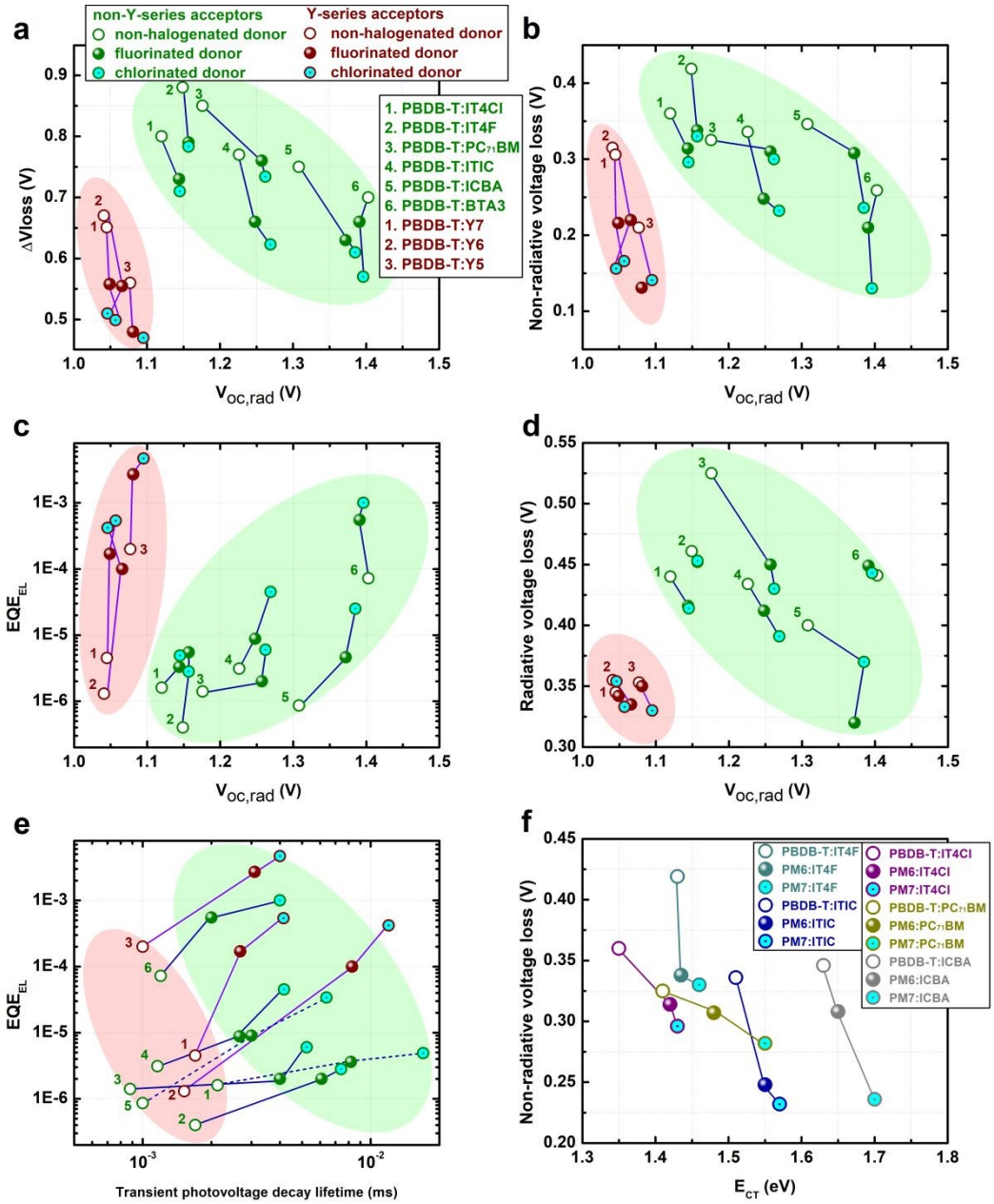

Figure 1. (a) ΔV_{loss} (defined as $\frac{E_g}{q} - V_{OC}$) as a function of $V_{oc,rad}$, **(b)** ΔV_{nr} (defined as $V_{oc,rad} - V_{OC}$) as a function of $V_{oc,rad}$, **(c)** EQE_{EL} as a function of $V_{oc,rad}$, **(d)** ΔV_r (defined as $\Delta V_{loss} - \Delta V_{nr}$) as a function of $V_{oc,rad}$, **(e)** EQE_{EL} as a function of transient photovoltage decay lifetime for the solar cells based on non-halogenated (open symbols) and halogenated (filled symbols) donors, mixed with the Y-series (red) and the non-Y-series (green) acceptors. **(f)** ΔV_{nr} as a function of E_{CT} for the solar cells based on the non-halogenated PBDB-T and the halogenated PM6, PM7, mixed with IT4F, ITIC, IT4Cl, $PC_{71}BM$, and ICBA. A summary of the voltage loss values for the solar cells is provided in **Table. S3 (Note S5, ESI)**.

To verify that the higher EQE_{EL} in the solar cells based on halogenated donors is indeed due to lower k_{nr}, transient photovoltage (TPV) decay measurements are performed. As expected, the transient photovoltage decay lifetime (**Figure 1e**), i.e., the lifetime of photo-generated charge carriers, closely related to the non-radiative decay dynamics of CT states,[43,47] is considerably longer in the solar cells based on halogenated donors, suggesting that k_{nr} is lower in the solar cells based on halogenated donors. Details regarding the TPV measurements are provided in **Note S6 (ESI)**.

As discussed above, in organic solar cells, k_{nr} is generally high because of the strong vibrational coupling between CT and ground state.[24] Since the degree of coupling is dependent on E_{CT}, k_{nr} is expected to exponentially increase with reducing E_{CT}, following the so-called energy gap law, i.e., ΔV_{nr} linearly increases with reducing E_{CT}.[24] To evaluate whether the increased E_{CT} after donor halogenation could be the reason for the reduced k_{nr}, highly sensitive EQE_{PV} and electroluminescence (EL) measurements are performed on semitransparent solar cells (to avoid interference of the spectra due to optics) with ITO as the bottom electrode and a 3 nm thick transparent Ag layer as the top electrode.[48,49] The results are shown in **Note S7 (ESI)**. From the EL spectra **(Figure S6**, **Note S7**, **ESI)**, we notice that for most of the solar cells based on the Y-series acceptors, the device emission is dominated by the S_1 state of the pure acceptor, due to the very small energetic driving force.[50] On the contrary, for the solar cells based on the non-Y series acceptors, including ITIC, IT4F, IT4Cl, $PC_{71}BM$, ICBA, mixed with halogenated or non-halogenated donors, the device emission is dominated by the CT state with photon energy lower than both the donor and the acceptor S_1 state energy (except for PM6:ITIC and PM7:ITIC). The presence of CT state emission allows us to derive the CT state properties, including E_{CT}, from the sensitive EQE_{PV} spectra **(Figure S7**, **Note S7**, **ESI)**, using the method described in the literature.[51] As summarized in **Figure 1f**, donor halogenation is confirmed to lead to increased E_{CT}, contributing to the reduction in k_{nr} and ΔV_{nr} in organic solar cells. However, the degree of reduction in ΔV_{nr} is in fact much higher than what was predicted by the energy gap law relation.[24] This indicates that the increased E_{CT} alone cannot explain the rapid decrease in k_{nr} and ΔV_{nr} in the solar cells after donor halogenation, and there must be an additional reason for the reduced k_{nr} and ΔV_{nr}.

In the framework of Marcus theory,[52] transfer rate between two states (k_{et}) can be expressed as[53]

View Article Online
DOI: 10.1039/D3EE00174A

$$k_{et} \propto V^2 FCWD(g) \quad (5)$$

where V is electronic coupling matrix element, related to the transition dipole moment, which is primarily determined by the transition oscillator strength. *FCWD(g)* is the Frank-Condon weighted density of states, exponentially dependent on the energy difference between the two states (g), as well as the reorganization energy associated with the transition. Thus, for CT state recombination in BHJ solar cells, apart from E_{CT}, the absorption oscillator strength of the CT state (f_{OSC}), the density of CT complex (N_{CTC}), and λ_{CT} are the most important parameters determining k_{nr}.[25] However, reducing f_{OSC} or N_{CTC} can lead to a reduction in both k_r and k_{nr},[25,54] meaning that EQE_{EL} of the solar cell does not necessarily change. Therefore, we conclude that the most likely reason for the reduced k_{nr} and ΔV_{nr} in the solar cells after donor halogenation is the reduced λ_{CT}. This will be discussed in more detail in the next section of this paper.

2.2. Impact of donor halogenation on the reorganization energies

To explain the reason for the reduced k_{nr} and ΔV_{nr} in the solar cells after donor halogenation, we focus on investigating the role that the donor halogenation strategy plays in determining the reorganization energy of the DA systems. For organic photovoltaic materials, there are two types of reorganization, namely, the high-frequency and the low-frequency reorganization. The high-frequency reorganization energy (λ^H) is attributed to the energy cost associated with the geometry change of the organic molecules from the optimized geometry in the ground state and the optimized geometry in the excited state[25,55,56]. The low-frequency reorganization energy (λ^L), on the other hand, is associated with the reorganization of the nuclear and dielectric environment to accommodate the charge-transfer processes. Thus, both λ^H and λ^L are highly critical in determining k_{nr} and ΔV_{nr} in organic solar cells.[25] A schematic illustration for the optical transitions between the excited and the ground states in organic materials is shown in **Figure 2a and 2b.** Accordingly, an expression for $FCWD(0)$ can be derived and put in equation (5) to obtain the non-radiative recombination rate constant,[25,55,57]

$$k_{nr} = \frac{2\pi}{\hbar} V^2 \frac{1}{\sqrt{4\pi\lambda_{CT}^L k_B T}} \sum_{w=0}^{\infty} \sum_{t=0}^{\infty} \frac{e^{-S} S^{w-t}}{w!} \left[L_t^{w-t}(S)\right]^2 e^{-\left\{\left[-E_{CT}+\lambda_{CT}^L+(w-t)\hbar\Omega\right]^2/4\lambda_{CT}^L k_B T\right\}} e^{-t\hbar\Omega/k_B T} \quad (6)$$

where λ_{CT}^L is the low-frequency reorganization energy of the CT states in the blend system, $\hbar$ is the reduced Planck constant, V is the electronic coupling between the CT and the ground state,

$S = \lambda_{CT}^{H}/\hbar\Omega$ is the Huang-Rhys factor,[58] λ_{CT}^{H} is the high-frequency reorganization energy of the CT state, Ω is the harmonic frequency of the quantized high-frequency mode, t and w represent the quantum number of the vibrational modes of the CT and the ground state, respectively, $L_t^{w-t}(S)$ is the generalized Laguerre polynomial at degree of t.

The overall CT state reorganization energies, λ_{CT}, of the DA blend systems depend on the reorganization energies of the neat materials.[59] Thus, the impact of donor halogenation on the reorganization energy of the model donor materials (λ_D), namely, the non-halogenated PBDB-T, and the halogenated PM6, PM7, is studied by performing PL measurements on the neat films. As shown in **Figure 2c**, the PL spectra of the films based on PBDB-T, as well as its halogenated derivatives, PM6 and PM7, can be deconvoluted into 4 peaks. Each peak corresponds to a specific transition from the vibrationally relaxed excited state to the ground state.[41] To evaluate the impact of donor halogenation on λ_D, the high intensity peaks (0-0 transitions) in the PL spectra are fitted using a Gaussian function, following the method described in the literature[41]. The Gaussian widths, corresponding to the low-frequency reorganization energy of the donor material (λ_D^L), were found to be similar for all of the films based on both halogenated and non-halogenated donors. More importantly, the ratio between the integrated area of the 0-0 transition peak and the integrated area of the complete spectrum (R_{00}) was determined to be higher for the films based on halogenated donors. The R_{00} ratios were 0.406, 0.319, and 0.274 for chlorinated PM7, fluorinated PM6, and non-halogenated PBDB-T, respectively. Because the 0-0 transition corresponds to the direct transition from the lowest vibrational level of the excited state to that of the ground state with minimum high-frequency molecular relaxation, a larger R_{00} indicates a smaller high-frequency reorganization energy of the donor material (λ_D^H). Thus, the λ_D^H is much lower in the films of the halogenated donors, as compared to that of the non-halogenated donor.

Accordingly, λ_D, and thus λ_{CT} for the blend active layer should also reduce after the donor halogenation. Indeed, when closely examining the fit parameters used for determining the E_{CT} of the solar cells (based on the DA systems with a large energetic driving force, see **Figure S7**, **Note S7**, **ESI)**, we find that λ_{CT} for the BHJ systems based on halogenated donors is generally lower, by as much as 0.1-0.3 eV, compared to that based on non-halogenated donors **(Figure 2d)**. The above results confirm that the lower k_{nr} in the solar cells based on halogenated donors is associated with

View Article Online
DOI: 10.1039/D3EE00174A

lower reorganization energy.

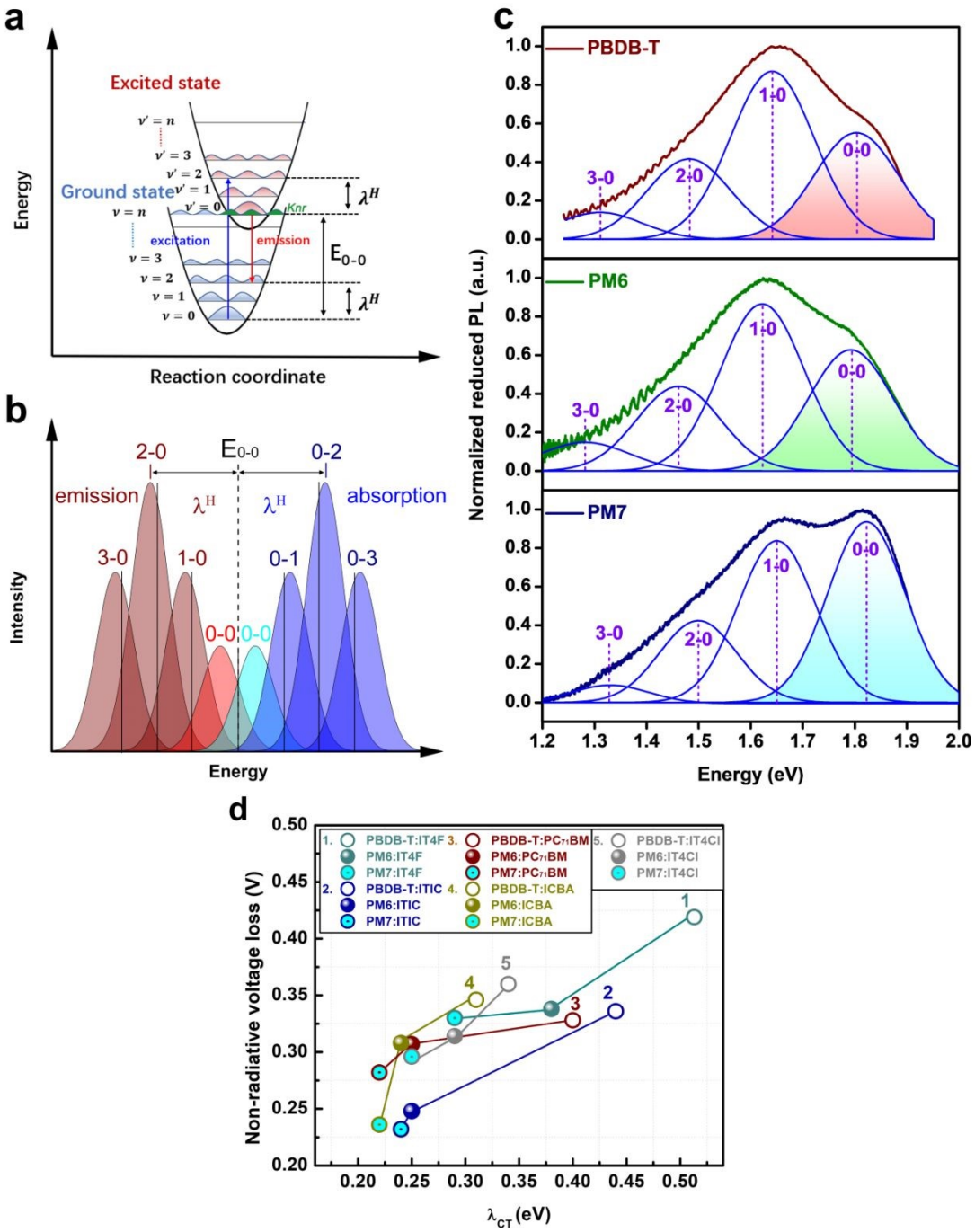

Figure 2. (a) Excited and ground state energy diagram for an organic semiconductor with discrete vibrational levels (v'=0, 1, 2, …). **(b)** Absorption and emission spectra of the organic semiconductor. The emission spectrum consists of a number of sub-peaks corresponding to different vibrational transitions. λ^L is related to the width of the sub-peaks, and λ^H is related to the ratio between the area of the 0-0 transition peak and the area of the full spectrum. **(c)** PL spectra of the thin films of neat non-halogenated PBDB-T, and halogenated PM6 and PM7, deconvoluted into discrete vibrational peaks that originate from the transitions from the relaxed excited state (v' = 0) to the different vibrational states in the ground state (v = 0, 1, 2, …). **(d)** ΔV_{nr} as a function of λ_{CT}. λ_{CT} values are determined from the sensitive EQE_{PV} spectra for the solar cells based on different active

View Article Online
DOI: 10.1039/D3EE00174A

materials systems.

To better understand the effect of halogenation on the CT state and on the recombination rate, we built a theoretical model of the PBDB-T:ITIC interface and its chlorinated counterpart, PM7:ITIC. The computational model of the PBDB-T and PM7 polymers consisted of a three-monomers oligomer. We remark that for PBDB-T and PM7 we used a simplified model that does not include the large paraffinic groups decorating the donor monomer (see **Figure 3a**). This simplification was necessary to make the problem computationally treatable (more details are provided in the experimental section). The PBDB-T and PM7 oligomers were put in contact with three ITIC molecules in a *face-on* configurations and the geometry of the system has been optimized at a density functional theory (DFT) level as described in detail in the experimental section. Starting from the ground state configurations, we optimized the geometry of the systems in the CT state at the same level of theory, i.e., based on time-dependent DFT (TD-DFT) using the same exchange and correlation functional and basis set. This approach is computationally expensive, beyond the complexity of calculations recently appeared in the literature,[27] but it guarantees a coherent and reliable evaluation of the CT characteristics. In **Figure 3a**, we show the electronic density difference between the ground and first excited state of the interface systems, illustrating the CT nature of the latter electronic state.

In qualitative agreement with the experiments (**Figure S7**, **Note S7**, **ESI**), calculations predict a 0.16 eV higher energy of the CT of the chlorinated system with respect to the reference one, with absolute values of 1.52 eV for the PM7:ITIC interface *vs.* 1.36 eV for PBTB-T:ITIC. Chlorination, however, has also an effect on the reorganization of the structure upon excitation in the CT state. Here, the reorganization energy of the non-radiative relaxation process is computed as the energy variation of the interface systems along the structural relaxation from the geometry corresponding to the vertical transition to the minimum energy in the arrival electronic state. In other words, λ_{CT}= $E_{GS} - E_{CT}$, where the subscript denotes the geometry in which the energy has been computed under CT state electronic level, GS standing for the optimal geometry in the electronic ground state and CT for the minimum energy geometry in the CT state. The advantage of computing the reorganization energy in the interface system, a more computationally expensive approach with respect to the standard one which is typically based on the GS and CT energetics of the individual molecules, is that it allows to consider possible constraints on structural changes upon electronic

excitation or relaxation due to the intermolecular interactions between the donor and acceptor. Our results are in agreement with experimental data, with a 0.09 eV reduction of the reorganization energy in PM7:ITIC (0.14 eV) with respect to PBDB-T:ITIC (0.23 eV).

The reduction of the reorganization energy arises from a minor distortion of both the donor and acceptor upon electronic excitation. An intuitive argument explaining the relation between molecular distortions upon non-radiative recombination, non-radiative recombination rate and the corresponding voltage losses can be drawn considering that the only non-negligible terms in the double sum of equation (6) are those associated to energy preserving vibronic transition. This implies that $w > t$, typically $w >> t$, which, according to the Fermi Golden rule and Frank-Condon theory, make transition between different vibrational states forbidden. Thus, structural distortions upon transition between the CT and ground electronic states make the Frank-Condon factor and the overlap integral between the initial and final vibration states non-zero, and the non-radiative recombination process possible (or more likely).

The difference of distortions between the two interfaces is shown in **Figure 3b**, in which we report the structure of the ground (blue) and CT (red) states of PBDB-T:ITIC and PM7:ITIC. The (minimalistic) stick representation is used to better highlight the differences. One notices that for the PM7:ITIC interface the ground and CT structures largely overlap, while in the PBDB-T:ITIC case one observes sizable differences between the two structures. To quantify these distortions we computed the root mean square displacement (RMSD) between the optimized structures of the ground and CT states of the PBDB-T:ITIC and PM7:ITIC interfaces, the average displacement of atoms in the configuration minima between the two electronic states. The RMSD of PBDB-T:ITIC is 0.75 Å, to be compared with a value of 0.28 Å of PM7:ITIC, which is consistent with the reduced reorganization energy of the interface including the halogenated donor. It is interesting to investigate the origin of this different RMSD. To this end, we computed the RMSD of the four molecules composing the computational sample, the donor oligomer and three molecules of the acceptor. To focus on the intramolecular distortions, we computed RMSD after the alignment of the individual molecules, i.e., after minimizing the RMSD between the ground state and CT geometry of each molecule upon their rotation/translation (see **Figure S8**, **Note S8**, **ESI**). The RMSD of the individual molecules are reported in **Table 1** and show that while the value of the PBDB-T:ITIC interface is

still larger than that of the PM7:ITIC counterpart, this difference is largely reduced with respect the overall value. Recalling that the difference between the *overall* and *molecule-by-molecule* RMSD is in the alignment, which is performed on the entire system in the first case, and individually for each molecule in the second, one must conclude that halogenation also reduces the distortion of the intermolecular arrangement of the interface upon electronic transition between the ground and CT states.

Table 1. Total and partial RMSD of the PBDB-T:ITIC and PM7:ITIC interfaces.

	PBDB-T:ITIC	PM7:ITIC
Total	0.75 Å	0.28 Å
Donor	0.45 Å	0.27 Å
Acceptor 1	0.49 Å	0.19 Å
Acceptor 2	0.23 Å	0.09 Å
Acceptor 3	0.12 Å	0.16 Å

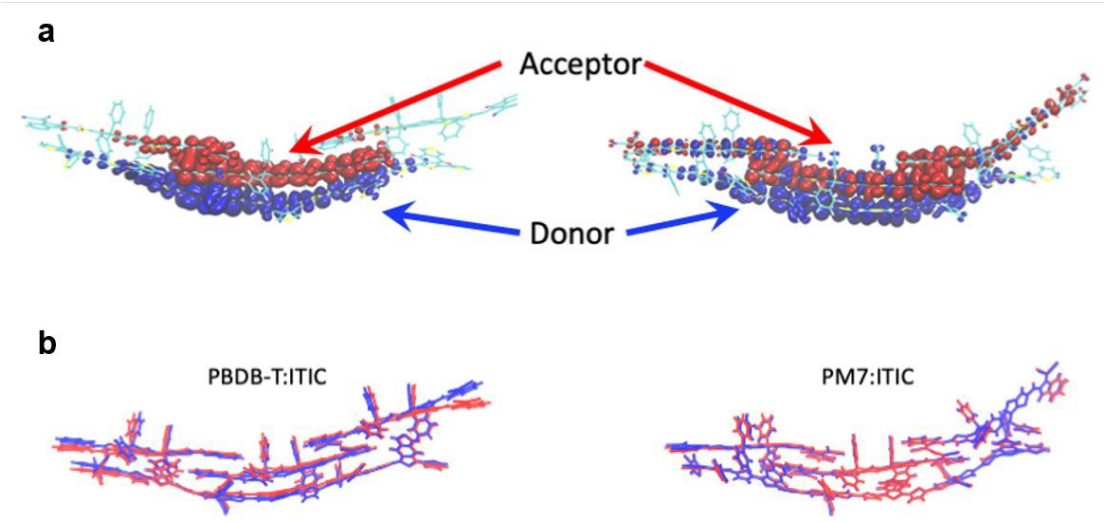

Figure 3. (a) Density difference between the ground and first excited state of the interface system. Red denotes an electronic density defect, and blue denotes an excess. This panel shows that the first excited state is, indeed, a charge transfer state. (**b)** Configuration of the PBDB-T:ITIC (left) and the PM7:ITIC (right) interfaces in the ground (blue) and CT (red) states. The figures have been drawn after alignment of the ground and CT state structures of the two interfaces. In the **Note S9 (ESI)**, we shown an analogous figure illustrating the structural differences between the ground and CT states of PBDB-T:ITIC and the PM7:ITIC focusing on individual molecules, after their alignment.

2.3. Origin of the different impact of the donor halogenation strategy on solar cells based on the Y-series and the non-Y-series acceptors

To comprehend the reason for the greater impact of the donor halogenation strategy on ΔV_{nr} of the solar cells based on the Y-series acceptors, as compared to that based on the non-Y-series acceptors, the effect of donor halogenation on the reorganization energy of the acceptor (λ_A) in the blends is also studied. First, the PL spectra of the blend films based on halogenated and non-halogenated donors mixed with the Y-series and the non-Y-series acceptors are measured. As shown in **Figure S9 (Note S9**, **ESI)**, the PL spectra of the blends based on the Y-series acceptors are dominated by the acceptor S_1 state emission, regardless of the donor used. This allows us to evaluate both the high-frequency (λ_A^H) and the low-frequency reorganization energy of the acceptor (λ_A^L) in the blends based on the Y-series acceptors (using the same method used for analyzing λ_D^H and λ_D^L of the neat donor materials). Using PBDB-T:Y6 as an example (**Figure 4a**), the λ_A^L of Y6 was found to be about 0.09 eV, similar to the λ_A^L in the blends based on the halogenated donors (0.10 and 0.11 eV for PM6:Y6 and PM7:Y6, respectively). Furthermore, R_{00} for the blend based on PBDB-T (0.67) was similar to that based on the halogenated donors (0.67 and 0.71 for PM6:Y6 and PM7:Y6, respectively). This suggests that λ_A^H of Y6 are similar in these blends. Accordingly, both λ_A^H and λ_A^L of Y6 in the blends, and thus, the packing properties of Y6 are hardly affected by the donor halogenation strategy.

On the contrary, for the blend films based on the non-Y-series acceptors, the PL emission spectra of most of the blends consist of both the donor and the acceptor S_1 state emission, except that for the blend based on IT4F. Thus, we deconvoluted the PL spectrum of PBDB-T:IT4F (**Figure 4b**), and determined λ_A^L for IT4F, which is 0.071 eV, similar to that in the blends based on the halogenated donors (0.073 and 0.079 eV for PM6:IT4F and PM7:IT4F, respectively). However, R_{00} is higher in the blend based on PBDB-T (0.58), compared to that based on the halogenated donors (0.50 and 0.51 for PM6:IT4F and PM7:IT4F, respectively). The lower R_{00} for the blends based on the halogenated donors indicate that λ_A^H of IT4F in the blends is increased by the halogenation of the donor. Therefore, λ_A of the blend is increased after donor halogenation.

For the blends based on IT4F, donor halogenation leads to reduced λ_D but increased λ_A. The degree of reduction in λ_{CT} after donor halogenation is likely limited. For the blends based on Y6,

donor halogenation reduces λ_D, but it does not affect λ_A. Thus, the degree of reduction in λ_{CT} after donor halogenation is expected to be higher for the blend based on Y6, compared to that based on IT4F. Therefore, we ascribe the greater impact of donor halogenation on ΔV_{nr} of the solar cells based on Y6, and by extension the Y-series acceptors, as compared to that based on the non-Y-series acceptors, to the higher degree of reduction in λ_{CT}.

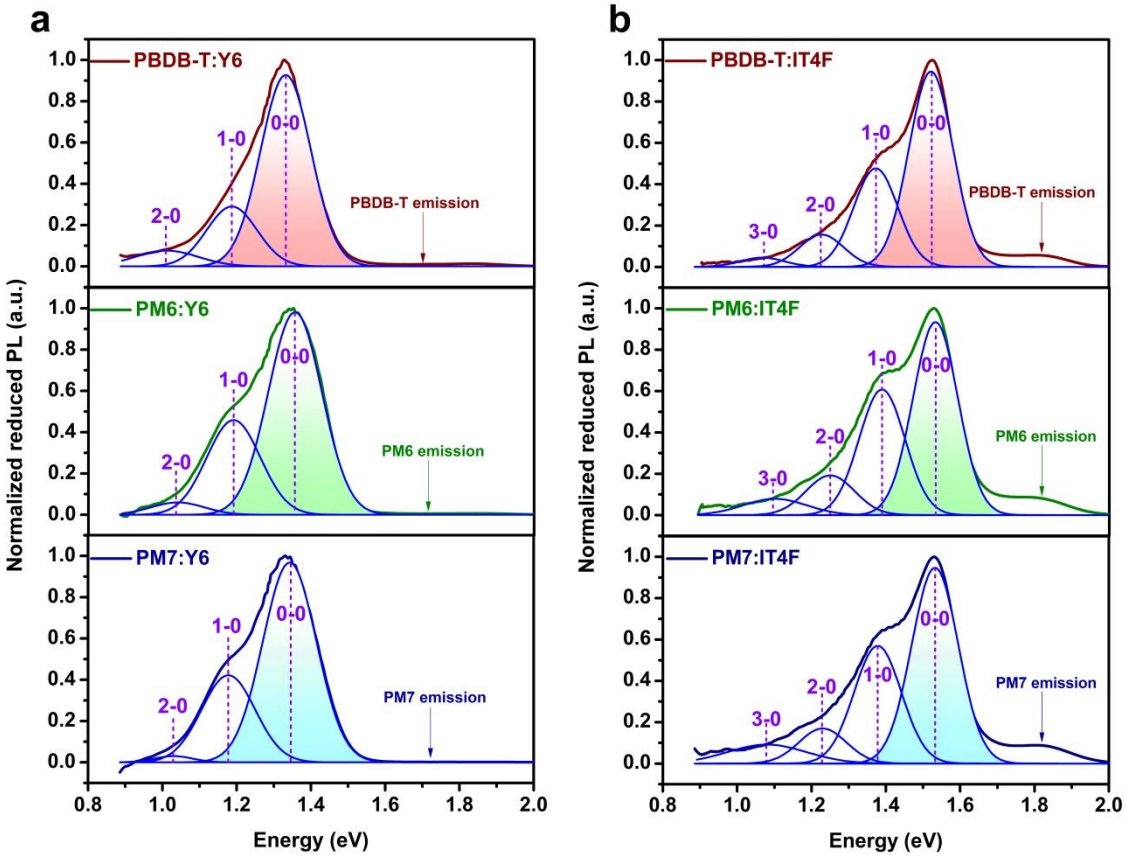

Figure 4. PL spectra of the blends films based on **(a)** PBDB-T:Y6, PM6:Y6, and PM7:Y6, and (**b)** PBDB-T:IT4F, PM6:IT4F, and PM7:IT4F. The PL spectra are dominated by the emission from the acceptors for these blend systems, and they are deconvoluted into a number of sub-peaks for the evaluation of λ_A^H and λ_A^L of the acceptors in the blend films.

2.4. The position of halogen substitution and its impact of ΔV_{nr} of organic solar cells

In theory, the position of halogenation plays a critically important role in determining the reorganization energy of organic systems.[60] To gain a better understanding of the optimal position for halogen substitution, the active material systems based on the model donors PBDB-T and PM7 (with chlorine substitution on the side thiophene units) were compared to the systems based on non-

halogenated PBT1-C and chlorine-substituted PBT1-C-2Cl (with chlorine substitution done on the polymer backbone).

The chemical structures of these materials are shown in **Figure 5a**. To achieve sufficiently high energetic driving force for the reliable determination of the CT state properties, including λ_{CT} and E_{CT}, IT4F is used as the acceptor for constructing semitransparent solar cells. The sensitive EQE_{PV} spectra are shown in **Figure 5b**. The λ_{CT} of the blend based on PBT1-C:IT4F does reduce after the backbone halogenation of the donor (**Figure 6a**). Nevertheless, the degree of reduction in λ_{CT} is considerably lower (from 0.40 to 0.33 eV), as compared to that realized for the systems based on PBDB-T (from 0.51 to 0.29 eV). Meanwhile, the backbone halogenation leads to significantly increased E_{CT} (from 1.40 to 1.49 eV) (**Figure 6b**). As a result, the reduced ΔV_{nr} in the solar cell after the backbone halogenation is primarily assigned to the increased E_{CT}. Similarly, for the solar cell based on PBDTT:IT4F (chemical structure shown in **Figure 5a**), the λ_{CT} is slightly reduced (0.44 to 0.42 eV) after the backbone halogenation (**Figure 5b**). Also, the reduced ΔV_{nr} is mainly due to the increase of E_{CT} from 1.24 to 1.37 eV (**Figure 6b**). Therefore, the origin of the reduced ΔV_{loss} for the solar cells after the backbone halogenation is very different from that for the solar cells after the side unit halogenation.

The impact of the side unit halogenation and the backbone halogenation is also investigated using molecular dynamic (MD) simulations, from which the radial distribution functions ($g(r)$) for the distances between centroids of conjugated structures of the donor and the acceptor materials are derived. More specifically, we use the centroids of the 1,3-bis(thiophen-2-yl)-5,7-bis(2-ethylhexyl)benzo-[1,2-c:4,5-*c*] dithiophene-4,8-dione (BDD) units of the donor material to represent the donor molecule, as the steric hinderance of the alkyl side chains on the 2-alkylthiophene-substituted benzo [1,2-b:4,5-*b'*] dithiophene (BDT) units of the donor molecules prevents close stacking between the BDT units and the acceptor molecules.[63] Details regarding the MD simulations are provided in **Note S10 (ESI)**. As shown in **Figure 7**, the closest distance between the donor and the acceptor molecules in the blend of PBDB-T:IT4F is estimated to be 5.50 Å, which is similar to that of PM7:IT4F with donor halogenation done on the side units. On the other hand, the distance of PBT-1-C:IT4F is 4.78 Å, which significantly increases (6.48 Å) after the backbone halogenation. It has been demonstrated that increasing the distance between the donor and the

acceptor molecules could give rise to increased E_{CT} of the donor-acceptor blend.[64,65] Thus, the higher degree of increase in E_{CT} for the blend after the backbone halogenation, as compared to that after the halogenation of the side unit, is ascribed to the increased donor-acceptor distance.

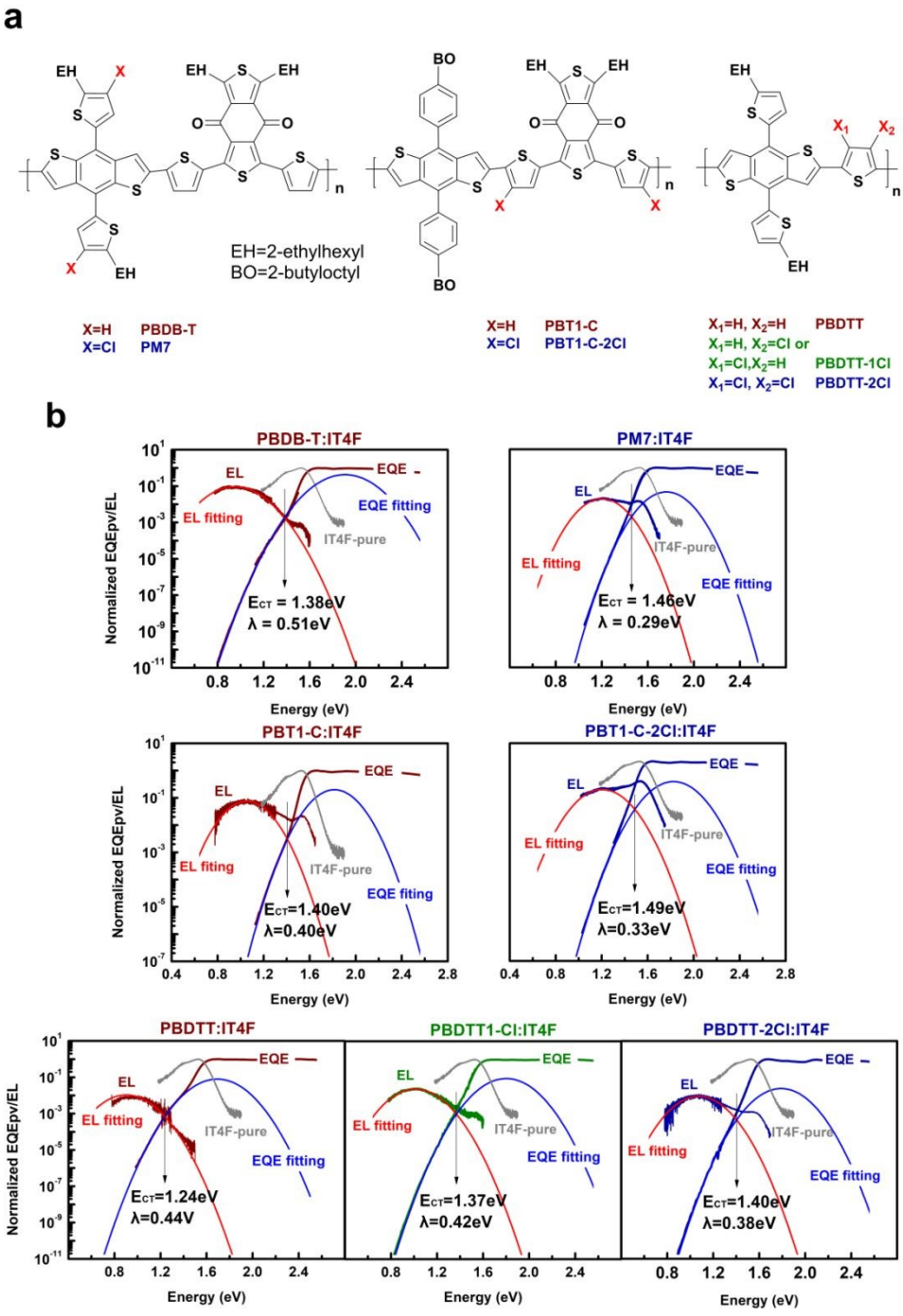

Figure 5. (a) Chemical structures of the donor materials PBDB-T, PM7, PBT1-C, PBT1-C-2Cl, PBDTT, PBDTT-1Cl, and PBDTT-2Cl. **(b)** Normalized sensitive EQE_{PV} and EL spectra for the solar cells based on the blend systems of PBDB-T, PM7, PBT1-C, PBT1-C-2Cl, PBDTT, PBDTT-1Cl, and PBDTT-2Cl, mixed with IT4F.

View Article Online
DOI: 10.1039/D3EE00174A

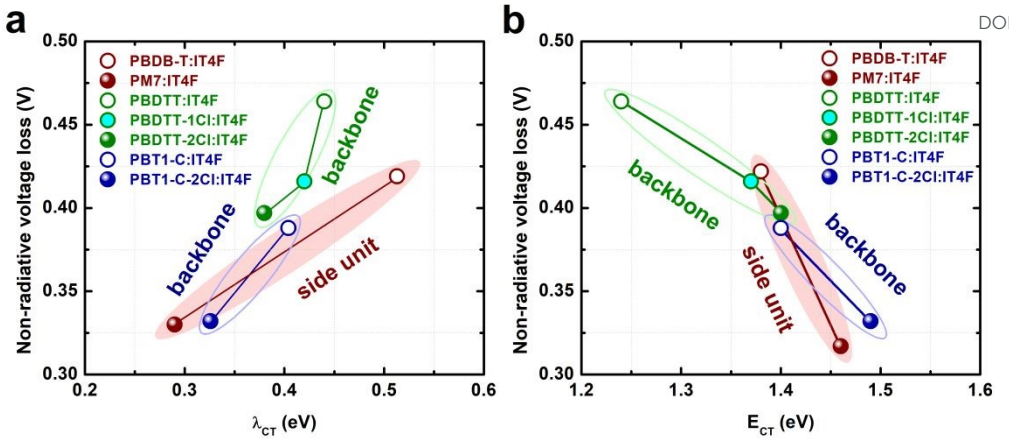

Figure 6. (a) ΔV_{nr} as a function of λ_{CT}, and **(b)** ΔV_{nr} as a function of E_{CT}, derived from the sensitive EQE_{PV} spectra of the solar cells.

Finally, we study the solar cells based on PBDTT-2Cl, with 2 chlorine atoms attached to the backbone of the donor, and we find that λ_{CT} is further reduced (**Figure 6a**), as compared to that of the non-halogenated donor PBDTT or the PBDTT-1Cl with one chlorine atom on the backbone. However, the addition of the chlorine atom also increases E_{CT}, being the main reason for the reduced ΔV_{nr}. MD simulations (**Figure 7c**) reveal that the DA distance does increase with the increasing number of chlorine atoms on the backbone. Therefore, it is concluded that the backbone halogenation of the donor mostly leads to increased E_{CT}, and the side unit halogenation of the donor is a more desired method to selectively reduce λ_{CT}, and thus, reduce ΔV_{loss} of organic solar cells.

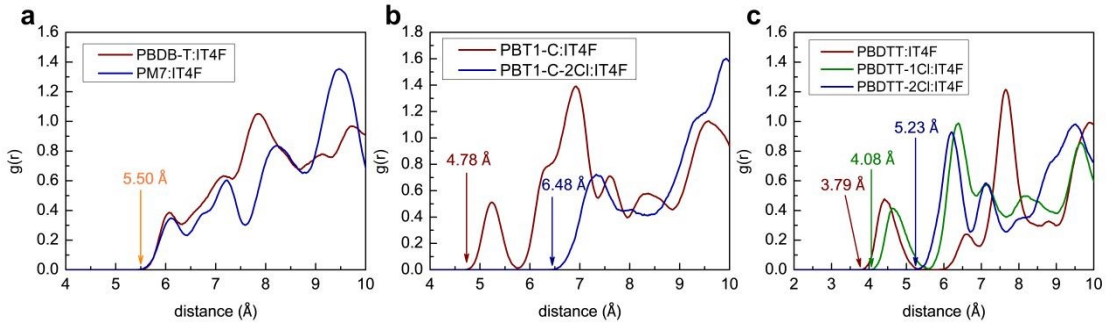

Figure 7. Radial distribution functions of the distances between the donor and acceptor molecules (represented by the centroids of the molecules) for the blends of **(a)** PBDB-T:IT4F and PM7:IT4F, **(b)** PBT1-C:IT4F and PBT1-C-2Cl:IT4F, and **(c)** PBDTT:IT4F, PBDTT-1Cl:IT4F, and PBDTT-2Cl:IT4F, determined from MD simulations.

View Article Online
DOI: 10.1039/D3EE00174A

3. Conclusion

In this work, over 30 donor-acceptor systems were investigated. The origin of the reduced voltage losses and improved device performance of organic solar cells after donor halogenation was partly attributed to the increased E_{CT}, and more importantly, to the reduced reorganization energy of the CT state. We demonstrated that for the blend systems based on non-Y-series acceptors, donor halogenation reduced the reorganization energy of the donor material, but increased the reorganization energy of the acceptor material. Nevertheless, the overall reorganization energy of the CT state was reduced after donor halogenation, leading to reduced ΔV_{nr}, and ΔV_{loss}. On the other hand, for the blend systems based on Y-series acceptors, donor halogenation also led to reduced reorganization energy of the donor, but it did not lead to increased acceptor reorganization energy. As a result, the degree of reduction in ΔV_{nr} after donor halogenation was higher for the solar cells based on Y-series acceptors, compared to those based on non-Y-series acceptors. This could be the main reason for the generally lower voltage loss and better performance of the solar cells based on halogenated donors mixed with Y-series acceptors. Additionally, we showed that the impact of the donor halogenation strategy on the reorganization energy of the CT state was dependent on the halogen substitution position, as well as the number of halogen atoms added to the donor molecule. Halogenation of the side units of the donor material could lead to significantly reduced reorganization energy of the CT state, but halogenation of the backbone mainly resulted in increased E_{CT} of the blend. As a result, halogenation of the side unit was found to be a more effective strategy for reducing the reorganization energy of the CT state. It is important to note that high ΔV_{loss} is currently a bottleneck in state-of-the-art organic solar cells, limiting their performance. Therefore, reducing ΔV_{loss} by reducing the reorganization energy of the CT state, as demonstrated in this work, is expected to be of great importance for further improved performance of organic solar cells.

View Article Online
DOI: 10.1039/D3EE00174A

4. Experiments and methods

Materials:

Polymer donors PBDB-T, PM6, and PM7, the non-Y series acceptors ITIC, IT4Cl, IT4F, and the Y-series acceptors Y5, Y6, Y7 were purchased from Solarmer materials Inc (China). $PC_{71}BM$ and ICBA were purchased from Solenne materials Inc. PBT1-C, PBT1-C-2Cl, PBDTT, PBDTT-1Cl, PBDTT-2Cl and BTA3 were synthesized according to the literature.[62,66,67] 1,8-diiodooctane (DIO), 1-chloronaphthalene (CN), chlorobenzene (CB), and chloroform (CF) were purchased from Sigma-Aldrich.

Fabrication of solar cells:

Organic solar cells with an inverted device architecture of ITO/ZnO/active layer/MoO_3/Ag were constructed in this work. The ITO glass substrates were cleaned with acetone, isopropanol, and ethanol solvent in sequence by an ultrasonic cleaner. Then, the surface of ITO substrates was treated by oxygen plasma for 10 minutes. ZnO precursor solution, prepared by the sol-gel method reported in the literature,[68] was deposited on the cleaned ITO substrates by spin-coating at 4000 rpm 60 s, the substrates were thermal annealed at 200 ℃ for 30 min. The thickness of the ZnO layers is about 30 nm, determined by a surface profilometer (KLA, Tencor P-7 Stylus Profiler).

The blend active layers based on the Y-series acceptors (Y5, Y6, Y7) (donor:acceptor weight ratio 1:1.2) were deposited on the ZnO coated substrates from chloroform solutions (with 0.5 vol% CN) in a nitrogen filled glovebox. The solutions were stirred on a hot plate (IKA RCT digital) at 55 ℃ for 4 hours prior to use. The concentration of the solutions was 16 mg mL^{-1}. The active layers were annealed at 90 °C for 5 min. The thickness of the active layers was about 90 nm, measured by a surface profilometer. The blend active layers based on the non-Y series acceptors (ITIC, IT4Cl, IT4F, and BTA3) (donor:acceptor weight ratio 1:1) were deposited on the ZnO coated substrates from chlorobenzene solutions (with 1 vol% DIO) in a nitrogen filled glovebox. The solutions were stirred on a hot plate (IKA RCT digital) at 80 ℃ for 4 hours, prior to use. The concentration of the solutions was 22 mg mL^{-1}. The active layers were annealed at 110 °C for 10 min. The thickness of the active layers was about 110 nm. The blend active layers based on the fullerene acceptors ($PC_{71}BM$, ICBA) (donor:acceptor weight ratio 1:1.2) were deposited on the ZnO coated substrates from chlorobenzene solutions (with 3 vol% DIO) in a nitrogen filled glovebox. The solutions were

View Article Online
DOI: 10.1039/D3EE00174A

stirred on a hot plate (IKA RCT digital) at 90 ℃ for 6 hours, prior to use. The concentration of the solutions was 25 mg mL^{-1}. The active layers were annealed at 100 °C for 10 min. The thickness of the active layers was about 110 nm. Then, the active layers were moved into a vacuum chamber (Mbraum), in which a 15 nm of MoO_3 and a 100 nm Ag layer were evaporated onto the active layers under a vacuum pressure of 10^{-6} mbar. The active area of the solar cells was 0.04 cm^2. For the semitransparent solar cells constructed in this work, a 15 nm MoO_3 and a 3 nm Ag layer are used as the top electrode.

Characterizations:

J-V Characterization. The performance parameters of the solar cells were acquired by using a Keithley 2400 source meter and simulated AM1.5G solar illumination (100 mW cm^{-2}) provided by a solar simulator (Newport Oriel VeraSol-2™ Class AAA). The solar simulator was calibrated by a standard silicon solar cell and a set of low-pass filters.

Highly Sensitive EQE_{PV} measurement. Sensitive EQE_{PV} spectra were measured by using monochromatic light from a halogen lamp light source (LSH-75, Newport) and a monochromator (CS260-RG-3-MC-A, Newport). A series of long-pass optical filters (600 nm, 900 nm, 1100 nm) were employed to eliminate the overtone wavelengths from the monochromator. The monochromatic light was chopped at a frequency of 173 Hz by an optical chopper (3502 Optical Chopper, Newport). A front-end current amplifier (SR570, Stanford Instrument) and a phase-locked amplifier (SR830, Stanford Instrument) were used to record the current signal from the solar cells. A Si detector (Hamamatsu s1337-1010BR) was used to calibrate the lamp intensity. The illuminated area is about 0.5 mm^2.

EQE_{EL} measurement. The EQE_{EL} measurements were done using a Keithley 2400 digital source meter to inject electrical current into the solar cells kept in dark. Emitted photons were recorded by a Si detector (Hamamatsu s1337-1010BR) and a Keithley 6482 Picoammeter.

EL measurement. Electroluminescence measurements were performed by injecting electric current (1 mA) into the device using a source meter (Keithley 2400). An optical fiber (BFL200LS02, Thorlab) was placed in front of the device to collect the photons emitted by the device. The emission spectra were recorded by a fluorescence spectrometer (KYMERA-328I-B2, Andor Technology) consists of two sets of gratings for the visible and the near-infrared spectral

range. A Si EMCCD detector (DU970P-BVF, Andor Technology) and an InGaAs detector (DU491A-1.7, Andor Technology) were used for recording the luminescence spectral ranges of 400~1000 nm and 900~1600 nm, respectively. The optical losses in the optical fiber, the spectrometer, and the detectors were corrected by a standard light source (Newport).

PL measurement. A super-continuous white laser (SuperK EXU-6, NKT photonics) and a laser narrowband filter (SR-VIS-HP8, NKT photonics) were used to excite the thin films. The excitation wavelength was 500 nm. Fluorescence signals from the organic films were recorded using the same setup used for the EL measurements.

TPV decay measurement. TPV measurement systems were done using a LED for the background illumination. The LED was controlled by a Keithley 2450. Another LED driven by an arbitrary function generator (AFG3022C, Tektronix) was used to generated pulsed illumination. The transient photovoltage signals of the devices were recorded by an oscilloscope (Tektronix, MDO4104C). The time interval between two adjacent pulses was set to be 5 microseconds. More specifically, the devices were placed under the bias LED illumination for the generation of the bias photovoltage close to the V_{OC} of the device under simulated AM1.5G illumination. Then, the pulsed LED illumination was added to generate an additional transient voltage in the device. The transient signal was set to be about 5% higher than the bias photovoltage, via controlling the intensity of pulsed illumination. To determine the transient photovoltage lifetime values for the devices under different illumination intensities, different injection currents were used to drive the bias LED.

Ab initio calculations. The two *face-on* model interfaces were prepared starting from the PBDB-T trimer and three ITIC molecules in their minimum energy configuration at a PBE0/D4 level of theory using a pcseg-1 basis set.[69–71] The overall PBDB-T:ITIC interface is further optimized and the same is done for the PM7:ITIC analogue, obtained by substituting selected hydrogen with chlorine atoms. Based on recent literature, the reorganization energy has been computed using the range separated revM11 exchange and correlation functional,[72] which is suitable to handle the energetics of long-range correlated systems.[56,73] Calculations have been performed using LSDalton and ORCA software.[74,75]

View Article Online
DOI: 10.1039/D3EE00174A

View Article Online
DOI: 10.1039/D3EE00174A

Conflicts of interest

There are no conflicts to declare.

Author Contributions

H.W., W.T., and Z.T. conceived the project. H.W. and M.L. fabricated and characterized the solar cells. H.W. and J.W. carried out the MD simulation. J.M.H.O. and S.M. performed DFT calculations. H.W. and M.L. performed the photoluminescence and transient photovoltage decay measurements. A.T. and E.Z. synthesized the acceptor BTA3. Y.S. synthesized the polymer donors PBT1-C and PBT1-C-2Cl. H.L. and Z.B. synthesized the polymer donors PBDTT, PBDTT-1Cl, and PBDTT-2Cl, and fabricated the devices based on PBDTT, PBDTT-1Cl, and PBDTT-2Cl. H.W., Z.M., W.T., J.M.H.O., S.M., and Z.T. wrote the manuscript. All authors contributed to the finalizing of the manuscript.

Acknowledgements

The work was financially supported by the National Natural Science Foundation of China (NSFC, Grant No. 51933001, 51973031, 52073056), the Natural Science Foundation of Shanghai (Grant No. 22ZR1401900), and the Fundamental Research Funds for the Central Universities (2232022A13, 2232021A09). S. M. acknowledges support from University of Ferrara "Fondo per l'Incentivazione alla Ricerca". J.M.H.O acknowledges financial support from VILLUM FONDEN (Grant No. 29478). W.T. acknowledges funding from the European Union's Horizon 2020 research and innovation program under grant agreement no. 851676 (ERC StGrt).

References

1 J. Wang, Z. Zheng, Y. Zu, Y. Wang, X. Liu, S. Zhang, M. Zhang and J. Hou, *Adv. Mater.*, 2021, **33**, 2102787.

2 L. Zhu, M. Zhang, J. Xu, C. Li, J. Yan, G. Zhou, W. Zhong, T. Hao, J. Song, X. Xue, Z. Zhou, R. Zeng, H. Zhu, C.-C. Chen, R. C. I. MacKenzie, Y. Zou, J. Nelson, Y. Zhang, Y. Sun and F. Liu, *Nat. Mater.*, 2022, **21**, 656–663.

3 Y. Cui, Y. Xu, H. Yao, P. Bi, L. Hong, J. Zhang, Y. Zu, T. Zhang, J. Qin, J. Ren, Z. Chen, C. He, X. Hao, Z. Wei and J. Hou, *Adv. Mater.*, 2021, **33**, 2102420.

4 R. Sun, Y. Wu, X. Yang, Y. Gao, Z. Chen, K. Li, J. Qiao, T. Wang, J. Guo, C. Liu, X. Hao, H. Zhu and J. Min, *Adv. Mater.*, 2022, **34**, 2110147.

5 Z. Zheng, J. Wang, P. Bi, J. Ren, Y. Wang, Y. Yang, X. Liu, S. Zhang and J. Hou, *Joule*, 2022, **6**, 171–184.
6 C. He, Y. Pan, Y. Ouyang, Q. Shen, Y. Gao, K. Yan, J. Fang, Y. Chen, C.-Q. Ma, J. Min, C. Zhang, L. Zuo and H. Chen, *Energy Environ. Sci.*, 2022, **15**, 2537–2544.
7 C. Li, J. Zhou, J. Song, J. Xu, H. Zhang, X. Zhang, J. Guo, L. Zhu, D. Wei, G. Han, J. Min, Y. Zhang, Z. Xie, Y. Yi, H. Yan, F. Gao, F. Liu and Y. Sun, *Nat. Energy*, 2021, **6**, 605–613.
8 J. Hou, O. Inganäs, R. H. Friend and F. Gao, *Nat. Mater.*, 2018, **17**, 119–128.
9 Z. Zheng, H. Yao, L. Ye, Y. Xu, S. Zhang and J. Hou, *Mater. Today*, 2020, **35**, 115–130.
10 Z. Zhou, W. Liu, G. Zhou, M. Zhang, D. Qian, J. Zhang, S. Chen, S. Xu, C. Yang, F. Gao, H. Zhu, F. Liu and X. Zhu, *Adv. Mater.*, 2020, **32**, 1906324.
11 Y. Wang, Y. Zhang, N. Qiu, H. Feng, H. Gao, B. Kan, Y. Ma, C. Li, X. Wan and Y. Chen, *Adv. Energy Mater.*, 2018, **8**, 1702870.
12 Y. Cui, H. Yao, J. Zhang, T. Zhang, Y. Wang, L. Hong, K. Xian, B. Xu, S. Zhang, J. Peng, Z. Wei, F. Gao and J. Hou, *Nat. Commun.*, 2019, **10**, 2515.
13 Q. Zhao, J. Qu and F. He, *Adv. Sci.*, 2020, **7**, 2000509.
14 H. Meng, Y. Li, B. Pang, Y. Li, Y. Xiang, L. Guo, X. Li, C. Zhan and J. Huang, *ACS Appl. Mater. Interfaces*, 2020, **12**, 2733–2742.
15 J. Cai, X. Zhang, C. Guo, Y. Zhuang, L. Wang, D. Li, D. Liu and T. Wang, *Adv. Funct. Mater.*, 2021, **31**, 2102189.
16 R. Ma, T. Liu, Z. Luo, Q. Guo, Y. Xiao, Y. Chen, X. Li, S. Luo, X. Lu, M. Zhang, Y. Li and H. Yan, *Sci. China Chem.*, 2020, **63**, 325–330.
17 J. Oh, K. Kranthiraja, C. Lee, K. Gunasekar, S. Kim, B. Ma, B. J. Kim and S.-H. Jin, *Adv. Mater.*, 2016, **28**, 10016–10023.
18 M. Zhang, X. Guo, S. Zhang and J. Hou, *Adv. Mater.*, 2014, **26**, 1118–1123.
19 A. C. Stuart, J. R. Tumbleston, H. Zhou, W. Li, S. Liu, H. Ade and W. You, *J. Am. Chem. Soc.*, 2013, **135**, 1806–1815.
20 H. Liu, M. Li, H. Wu, J. Wang, Z. Ma and Z. Tang, *J. Mater. Chem. A*, 2021, **9**, 19770–19777.
21 N. An, Y. Cai, H. Wu, A. Tang, K. Zhang, X. Hao, Z. Ma, Q. Guo, H. S. Ryu, H. Y. Woo, Y. Sun and E. Zhou, *Adv. Mater.*, 2020, **32**, 2002122.
22 R. Lenaerts, D. Devisscher, G. Pirotte, S. Gielen, S. Mertens, T. Cardeynaels, B. Champagne, L. Lutsen, D. Vanderzande, P. Adriaensens, P. Verstappen, K. Vandewal and W. Maes, *Dyes Pigm.*, 2020, **181**, 108577.
23 A. Tang, W. Song, B. Xiao, J. Guo, J. Min, Z. Ge, J. Zhang, Z. Wei and E. Zhou, *Chem. Mater.*, 2019, **31**, 3941–3947.
24 J. Benduhn, K. Tvingstedt, F. Piersimoni, S. Ullbrich, Y. Fan, M. Tropiano, K. A. McGarry, O. Zeika, M. K. Riede, C. J. Douglas, S. Barlow, S. R. Marder, D. Neher, D. Spoltore and K. Vandewal, *Nat. Energy*, 2017, **2**, 17053.
25 M. Azzouzi, J. Yan, T. Kirchartz, K. Liu, J. Wang, H. Wu and J. Nelson, *Phys. Rev. X*, 2018, **8**, 031055.
26 X. Chen and J. Brédas, *Adv. Energy Mater.*, 2018, **8**, 1702227.
27 D. Qian, Z. Zheng, H. Yao, W. Tress, T. R. Hopper, S. Chen, S. Li, J. Liu, S. Chen, J. Zhang, X.-K. Liu, B. Gao, L. Ouyang, Y. Jin, G. Pozina, I. A. Buyanova, W. M. Chen, O. Inganäs, V. Coropceanu, J.-L. Bredas, H. Yan, J. Hou, F. Zhang, A. A. Bakulin and F. Gao, *Nat. Mater.*, 2018, **17**, 703–709.

28 J. Yuan, Y. Zhang, L. Zhou, C. Zhang, T. Lau, G. Zhang, X. Lu, H. Yip, S. K. So, S. Beaupré, M. Mainville, P. A. Johnson, M. Leclerc, H. Chen, H. Peng, Y. Li and Y. Zou, *Adv. Mater.*, 2019, **31**, 1807577.

29 J. Yuan, Y. Zhang, L. Zhou, G. Zhang, H.-L. Yip, T.-K. Lau, X. Lu, C. Zhu, H. Peng, P. A. Johnson, M. Leclerc, Y. Cao, J. Ulanski, Y. Li and Y. Zou, *Joule*, 2019, **3**, 1140–1151.

30 T. Liu, Y. Zhang, Y. Shao, R. Ma, Z. Luo, Y. Xiao, T. Yang, X. Lu, Z. Yuan, H. Yan, Y. Chen and Y. Li, *Adv. Funct. Mater.*, 2020, **30**, 2000456.

31 M. Zhang, X. Guo, W. Ma, H. Ade and J. Hou, *Adv. Mater.*, 2015, **27**, 4655–4660.

32 S. Zhang, Y. Qin, J. Zhu and J. Hou, *Adv. Mater.*, 2018, **30**, 1800868.

33 G. Zhang, X.-K. Chen, J. Xiao, P. C. Y. Chow, M. Ren, G. Kupgan, X. Jiao, C. C. S. Chan, X. Du, R. Xia, Z. Chen, J. Yuan, Y. Zhang, S. Zhang, Y. Liu, Y. Zou, H. Yan, K. S. Wong, V. Coropceanu, N. Li, C. J. Brabec, J.-L. Bredas, H.-L. Yip and Y. Cao, *Nat. Commun.*, 2020, **11**, 3943.

34 X.-K. Chen, D. Qian, Y. Wang, T. Kirchartz, W. Tress, H. Yao, J. Yuan, M. Hülsbeck, M. Zhang, Y. Zou, Y. Sun, Y. Li, J. Hou, O. Inganäs, V. Coropceanu, J.-L. Bredas and F. Gao, *Nat. Energy*, 2021, **6**, 799-806.

35 A. Karki, J. Vollbrecht, A. L. Dixon, N. Schopp, M. Schrock, G. N. M. Reddy and T. Nguyen, *Adv. Mater.*, 2019, **31**, 1903868.

36 F. D. Eisner, M. Azzouzi, Z. Fei, X. Hou, T. D. Anthopoulos, T. J. S. Dennis, M. Heeney and J. Nelson, *J. Am. Chem. Soc.*, 2019, **141**, 6362–6374.

37 Y. Lin, J. Wang, Z.-G. Zhang, H. Bai, Y. Li, D. Zhu and X. Zhan, *Adv. Mater.*, 2015, **27**, 1170–1174.

38 W. Zhao, S. Li, H. Yao, S. Zhang, Y. Zhang, B. Yang and J. Hou, *J. Am. Chem. Soc.*, 2017, **139**, 7148–7151.

39 H. Zhang, H. Yao, J. Hou, J. Zhu, J. Zhang, W. Li, R. Yu, B. Gao, S. Zhang and J. Hou, *Adv. Mater.*, 2018, **30**, 1800613.

40 D. Qian, L. Ye, M. Zhang, Y. Liang, L. Li, Y. Huang, X. Guo, S. Zhang, Z. Tan and J. Hou, *Macromolecules*, 2012, **45**, 9611–9617.

41 K. Vandewal, J. Benduhn and V. C. Nikolis, *Sustainable Energy Fuels*, 2018, **2**, 538–544.

42 U. Rau, *Phys. Rev. B*, 2007, **76**, 085303.

43 K. Vandewal, *Annu. Rev. Phys. Chem.*, 2016, **67**, 113–133.

44 K. Vandewal, S. Albrecht, E. T. Hoke, K. R. Graham, J. Widmer, J. D. Douglas, M. Schubert, W. R. Mateker, J. T. Bloking, G. F. Burkhard, A. Sellinger, J. M. J. Fréchet, A. Amassian, M. K. Riede, M. D. McGehee, D. Neher and A. Salleo, *Nat. Mater.*, 2014, **13**, 63–68.

45 X.-K. Chen, M. K. Ravva, H. Li, S. M. Ryno and J.-L. Brédas, *Adv. Energy Mater.*, 2016, **6**, 1601325.

46 X. Liu, Y. Li, K. Ding and S. Forrest, *Phys. Rev. Applied*, 2019, **11**, 024060.

47 O. J. Sandberg and A. Armin, *J. Phys. Chem. C*, 2021, **125**, 15590–15598.

48 T. Schwab, S. Schubert, L. Müller-Meskamp, K. Leo and M. C. Gather, *Adv. Opt. Mater.*, 2013, **1**, 921–925.

49 A. Armin, N. Zarrabi, O. J. Sandberg, C. Kaiser, S. Zeiske, W. Li and P. Meredith, *Adv. Energy Mater.*, 2020, **10**, 2001828.

50 L. Perdigón-Toro, L. Q. Phuong, S. Zeiske, K. Vandewal, A. Armin, S. Shoaee and D. Neher, *ACS Energy Lett.*, 2021, **6**, 557–564.

51 K. Vandewal, K. Tvingstedt, A. Gadisa, O. Inganäs and J. V. Manca, *Phys. Rev. B*, 2010, **81**, 125204.
52 R. A. Marcus, *Rev. Mod. Phys.*, 1993, **65**, 599–610.
53 I. R. Gould, D. Noukakis, L. Gomez-Jahn, R. H. Young, J. L. Goodman and S. Farid, *Chem. Phys.*, 1993, **176**, 439–456.
54 K. Vandewal, J. Widmer, T. Heumueller, C. J. Brabec, M. D. McGehee, K. Leo, M. Riede and A. Salleo, *Adv. Mater.*, 2014, **26**, 3839–3843.
55 P. F. Barbara, T. J. Meyer and M. A. Ratner, *J. Phys. Chem.*, 1996, **100**, 13148–13168.
56 V. Coropceanu, X.-K. Chen, T. Wang, Z. Zheng and J.-L. Brédas, *Nat. Rev. Mater.*, 2019, **4**, 689–707.
57 J. Jortner, *J. Chem. Phys.*, 1976, **64**, 4860–4867.
58 K. Huang, R. Avril, *Proc. R. Soc. Lond. A*, 1950, **204**, 406–423.
59 K. Vandewal, J. Benduhn, K. S. Schellhammer, T. Vangerven, J. E. Rückert, F. Piersimoni, R. Scholz, O. Zeika, Y. Fan, S. Barlow, D. Neher, S. R. Marder, J. Manca, D. Spoltore, G. Cuniberti and F. Ortmann, *J. Am. Chem. Soc.*, 2017, **139**, 1699–1704.
60 H. Geng, Y. Niu, Q. Peng, Z. Shuai, V. Coropceanu and J.-L. Brédas, *J. Chem. Phys.*, 2011, **135**, 104703.
61 T. Liu, L. Huo, S. Chandrabose, K. Chen, G. Han, F. Qi, X. Meng, D. Xie, W. Ma, Y. Yi, J. M. Hodgkiss, F. Liu, J. Wang, C. Yang and Y. Sun, *Adv. Mater.*, 2018, **30**, 1707353.
62 L. Ye, Y. Xie, K. Weng, H. S. Ryu, C. Li, Y. Cai, H. Fu, D. Wei, H. Y. Woo, S. Tan and Y. Sun, *Nano Energy*, 2019, **58**, 220–226.
63 G. Han, Y. Guo, X. Ma and Y. Yi, *Sol. RRL*, 2018, **2**, 1800190.
64 J. Wang, X. Jiang, H. Wu, G. Feng, H. Wu, J. Li, Y. Yi, X. Feng, Z. Ma, W. Li, K. Vandewal and Z. Tang, *Nat. Commun.*, 2021, **12**, 6679.
65 J. Liu, Y. Zhang, P. Bao and Y. Yi, *J. Chem. Theory Comput.*, 2017, **13**, 843–851.
66 B. Xiao, A. Tang, Q. Zhang, G. Li, X. Wang and E. Zhou, *ACS Appl. Mater. Interfaces*, 2018, **10**, 34427–34434.
67 H. Wang, H. Lu, Y. Chen, G. Ran, A. Zhang, D. Li, N. Yu, Z. Zhang, Y. Liu, X. Xu, W. Zhang, Q. Bao, Z. Tang and Z. Bo, *Adv. Mater.*, 2022, **34**, 2105483.
68 Y. Sun, J. H. Seo, C. J. Takacs, J. Seifter and A. J. Heeger, *Adv. Mater.*, 2011, **23**, 1679–1683.
69 E. Caldeweyher, S. Ehlert, A. Hansen, H. Neugebauer, S. Spicher, C. Bannwarth and S. Grimme, *J. Chem. Phys.*, 2019, **150**, 154122.
70 E. Caldeweyher, C. Bannwarth and S. Grimme, *J. Chem. Phys.*, 2017, **147**, 034112.
71 C. Adamo and V. Barone, *The Journal of Chemical Physics*, 1999, **110**, 6158–6170.
72 P. Verma, Y. Wang, S. Ghosh, X. He and D. G. Truhlar, *J. Phys. Chem. A*, 2019, **123**, 2966–2990.
73 L. Benatto, M. de J. Bassi, L. C. W. de Menezes, L. S. Roman and M. Koehler, *J. Mater. Chem. C*, 2020, **8**, 8755–8769.
74 F. Neese, *WIREs Comput Mol. Sci.*, 2012, **2**, 73–78.
75 F. Neese, *WIREs Comput Mol. Sci.*, 2018, **8**, e1327.